Highly Conductive Ribbons Prepared by Stick–Slip Assembly of Organosoluble Gold Nanoparticles

Jimmy Lawrence, Jonathan T. Pham, Dong Yun Lee, Yujie Liu, Alfred J. Crosby,* and Todd Emrick*

Department of Polymer Science and Engineering, University of Massachusetts, Amherst, Massachusetts 01003, United States

ABSTRACT Precisely positioning and assembling nanoparticles (NPs) into hierarchical nanostructures is opening opportunities in a wide variety of applications. Many techniques employed to produce hierarchical micrometer and nanoscale structures are limited by complex fabrication of templates and difficulties with scalability. Here we describe the fabrication and characterization of conductive nanoparticle ribbons prepared from surfactant-free organosoluble gold nanoparticles (Au NPs). We used a flow-coating technique in a controlled, stick–slip assembly to regulate the deposition of Au NPs into densely packed, multilayered structures. This affords centimeter-scale long, high-resolution Au NP ribbons with precise periodic spacing in a rapid manner, up to 2 orders-of-magnitude finer and faster than previously reported methods. These Au NP ribbons exhibit linear ohmic response, with conductivity that varies by changing the binding headgroup of the ligands. Controlling NP percolation during sintering (*e.g.*, by adding polymer to retard rapid NP coalescence) enables the formation of highly conductive ribbons, similar to thermally sintered conductive adhesives. Hierarchical, conductive Au NP ribbons represent a promising platform to enable opportunities in sensing, optoelectronics, and electromechanical devices.

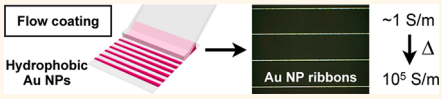

KEYWORDS: directed assemblies · nanomaterials · organosoluble nanoparticles · nanoparticle ribbons · conductive nanostructures

Precisely positioning and assembling nanoparticles (NPs) into well-defined nanostructures is opening new opportunities in electronics, optics, and sensing applications. However, there remain considerable challenges in nanoparticle research with regard to assembly methods.[1] Prior studies have reported nanoparticle positioning by conventional lithography, dip-pen nanolithography, e-jet printing, and various other writing techniques to produce micrometer and nanoscale structures.[2−4] However, these techniques are often limited by complex fabrication requirements of lithographic templates and substrates, as well as problems associated with scalability and fabrication time.[1]

Regulating the dynamic self-assembly of NPs is highly desirable because it offers an easy, inexpensive, and lithography-free route to produce well-defined nanostructures.[5] We recently showed that CdSe quantum dots (QDs), coated with their native alkane-based ligands (*i.e.*, tri-*n*-octylphosphine oxide and related ligands), are well-suited for preparing NP-based ribbons (termed "ribbons" since their width-to-height ratio is ∼30 or greater). These NP-ribbons were produced by flow coating: a rapid convective-driven assembly that combines the evaporative deposition of organosoluble NPs with capillary forces.[6,7] Grids and cross-linked NP ribbons were prepared by flow coating QDs functionalized with cross-linkable ligands, giving robust structures that maintain their structural integrity on substrates and when suspended in liquids. Here we build upon this NP fabrication platform to obtain fully functional (conductive) nanoparticle ribbons by tailoring the surface properties of organosoluble Au NPs.

Several reports describe the use of gold nanoparticles (Au NPs) as conductive NP building blocks,[8−10] such as by evaporative assembly from aqueous solutions of citrate-stabilized Au NPs deposited on a glass substrate by vertical colloidal deposition (VCD).[9] Au NP wires prepared by this technique are large, typically 5−180 μm in width and 100 nm in height.[10] In a recent study, Ressier *et al.* fabricated Au NP wires from citrate-stabilized Au NPs by convective self-assembly (CSA) obtaining Au NP wires several micrometers in width and <100 nm in height.[11] Although VCD and CSA allow for the facile formation of Au NP wires, these processes are time-consuming

* Address correspondence to crosby@mail.pse.umass.edu, tsemrick@mail.pse.umass.edu.

Received for review June 25, 2013 and accepted January 6, 2014.

Published online January 13, 2014
10.1021/nn4057726

(meniscus velocity: ~0.004 mm/s), do not allow precise control over spacing between NP wires, and require the use of water-soluble NPs. The flow coating we describe is significantly faster (meniscus velocity: 1.5 mm/s), allows precise control over spacing between NP ribbons (μm resolution), and exploits organosoluble NPs.

Since Brust reported the preparation of dodecanethiol-stabilized Au NPs using a two-phase method,[12] significant efforts have been devoted to the structure–property relationships of organosoluble Au NPs using Langmuir monolayers,[13−15] clusters,[16,17] crystalline aggregates,[8,18] and directed assembly.[10,11,19] In this study, we prepared Au NP ribbons from organosoluble Au NPs and study their morphologies and electrical properties. Interestingly, we could not prepare well-defined NP ribbons from dodecanethiol-stabilized Au NPs prepared by the standard Brust two-phase method, despite the facile formation of well-defined NP ribbons from CdSe QDs prepared by standard syntheses.[20,21] As shown below, the ligand density, nanoparticle size dispersity, and surfactant contamination should be considered for preparing well-defined Au NP ribbons. We found the Au NP ribbons to be conductive over substantial length scales, confirming the excellent fidelity of this flow coating methodology, and advancing the understanding of nanoparticle assembly to make functional nanostructures. The striking differences from previous works on Au NP assembly and patterning include the simplicity of the process (it resembles the widely implemented screen printing process, but does not require templates), the 2 orders of magnitude shorter time scale required to prepare high resolution NP ribbons using hydrophobic NPs, the extreme length of the conductive Au NP ribbons (~cm), and the efficient use of NPs (orders of magnitude less than inkjet or spin coating process).

RESULTS AND DISCUSSION

We examined Au NP samples prepared by different synthetic routes for NP deposition by flow coating. First we describe our use of three dodecanethiol-stabilized Au NP samples: **Au NP-1**, **Au NP-2**, and **Au NP-3**. **Au NP-1** was synthesized by a one-phase method[17] and **Au NP-2** by the Brust two-phase method,[12] while **Au NP-3** was a commercial sample obtained from Ocean Nanotech LLC (AuO-05-0025) (see the Supporting Information for the details of Au NP synthesis). Later, we describe the use of two additional samples, dodecylamine-stabilized **Au NP-4**, prepared by a one-phase method,[22] and **Au NP-5**, a mixture of **Au NP-4** with polystyrene. X-ray photoelectron spectroscopy (XPS) of **Au NP-1** and **Au NP-2** samples did not detect reaction by-products (*i.e.*, triphenylphospine for **Au NP-1** and tri-*n*-octylammonium bromide (TOAB) for **Au NP-2**). UV–vis spectra and TEM images of **Au NP-1** and **Au NP-2** are shown in Figure 1. A well-defined surface

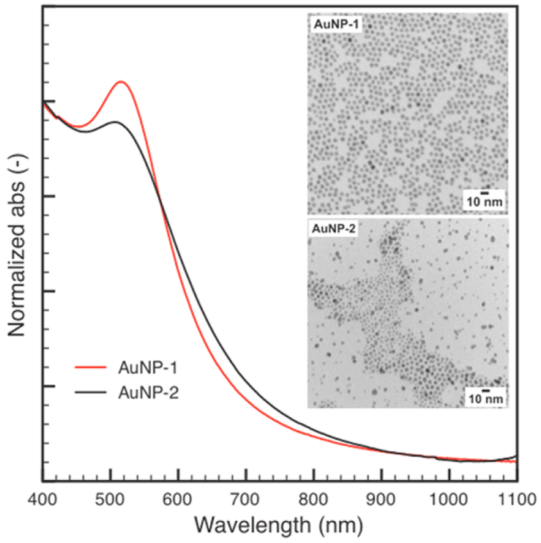

Figure 1. UV–vis spectra and TEM images of Au NP-1 and Au NP-2. Inset: TEM images of Au NP-1 and Au NP-2.

plasmon resonance (SPR) for each sample at 520 nm confirmed their narrow size dispersity. TEM analysis showed **Au NP-1** to be 5.0 ± 0.5 nm and **Au NP-2** to be 3.8 ± 1.3 nm. The commercial Au NPs used in this study (**Au NP-3**) were also of narrow dispersity (5.1 ± 0.7 nm).

Au NP ribbons on glass substrates were prepared from these three samples by flow coating, and their optical microscopy images are shown in Figure 2. In a typical experiment, a dilute solution of Au NPs (1 mg/mL, [Au $NP_{5\ nm}$] = 1.3 μM) is introduced between a flexible coating blade and the underlying substrate (Figure 2a). Capillary forces trap the NP solution under the blade, and solvent evaporation drives the NPs to the contact line. Following a prescribed deposition time to form an individual ribbon, the substrate is translated to stretch the meniscus and move the contact line to a new position. As seen qualitatively in Figure 2b, the quality of the Au NP ribbons obtained from **Au NP-1** solutions was much better than those from **Au NP-2** and **Au NP-3** solutions. Later, we show that higher quality Au NP ribbons exhibit better continuity and conductivity and are not disrupted significantly by surface dewetting. We found that the quality of **Au NP-1** ribbons was not affected by varying the deposition time. In **Au NP-2** ribbon arrays, the effect of periodic fingering instabilities (likely Marangoni instabilities[23,24]) became pronounced when deposition time was decreased from 1 to 0.5 s (Figure 2b). For **Au NP-3** ribbons, similar instabilities were observed.

We hypothesized that the quality of Au NP ribbons might be improved by adjusting their surface energy by decreasing ligand density on the NP surface. A lower ligand density would also reduce interparticle distance in the deposited structures and potentially improve conductivity.[25,26] Surfactant-free Au NP syntheses proved useful, since the surface energy of the

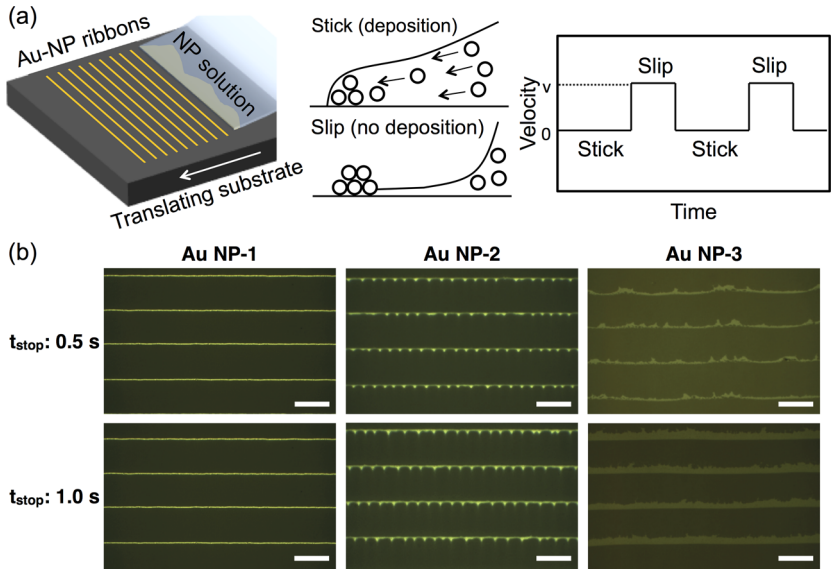

Figure 2. (a) Schematic illustration of the preparation of Au NP ribbons by flow coating, showing the stick-and-slip deposition of Au NPs as the stage was translated and the velocity profile of the stage translation. (b) Optical microscopy (OM) images of Au NP ribbons prepared by flow-coating (left to right: Au NP-1, Au NP-2, and Au NP-3). Au NP ribbons were deposited with various deposition time (given in the left of each micrograph row as t_{stop}). Scale bar in each image is 20 μm.

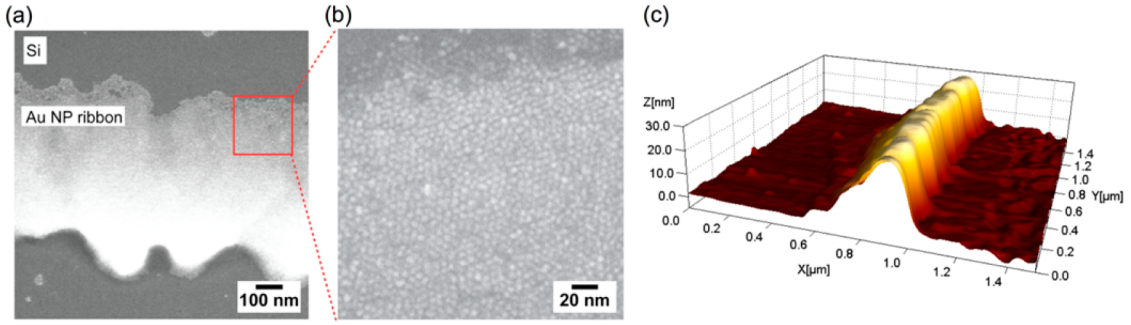

Figure 3. (a) SEM image of a ribbon prepared from Au NP-1 on a Si substrate. (b) Magnified SEM image showing individual densely packed Au NPs. (c) AFM 3D image (height mode) of a Au NP-1 ribbon.

NP-solvent interface is important for controlling line fidelity. Indeed, adopting surfactant-free synthesis[27] was crucial for the successful fabrication of Au NP ribbons.

The ligand density (normalized for NP surface area) of each Au NP sample was calculated from the organic weight percent of the sample determined by TGA and the NP diameter determined by TEM. This gave ligand densities of 7.1, 8.0, and 8.6 molecules/nm^2 for **Au NP-1**, **Au NP-2**, and **Au NP-3**, respectively. Even the modest reduction in ligand density of **Au NP-1** compared to **Au NP-2** (12% less) and **Au NP-3** (18% less) evidently had a substantial impact on the quality of the NP ribbons. XPS characterization indicated a higher carbon-to-thiol ratio for **Au NP-2** and **Au NP-3** samples relative to **Au NP-1**, suggesting the presence of nonthiol-contaminant on **Au NP-2** and **Au NP-3** surfaces (see the Supporting Information, **Table SI-1**). Since using NPs with depleted ligand coverage and/or free of surfactants proved crucial to successful production of high quality Au NP ribbon arrays, the structural and electrical characterizations that follow were performed on NP ribbons prepared from **Au NP-1**.

Figure 3 shows SEM and AFM images of Au NP-1 ribbon arrays obtained on Si substrates. Figure 3a is an SEM image of a single Au NP ribbon, and Figure 3b shows a magnified image of an area within the ribbon, in which individual Au NPs (diameter: ~5 nm) are seen as a densely packed multilayer. The nanometer-scale waviness at the ribbon edge was presumably the result of modest periodic fingering instabilities. The width of the ribbons seen by SEM was ~600 nm. Cross-sectional AFM images of the Au NP ribbons showed their width and height to be in the range of 500−700 and 30−50 nm, respectively. The height of Au NP ribbons obtained by flow coating is comparable to previous reports on Au wires prepared from aqueous solution of citrate-stabilized Au NPs,[10,11] but the ribbon width obtained by our method is 1−2 orders of magnitude smaller. As such, our results showed that flow coating is useful to "write" organosoluble conductive elements with fine features and tailorable patterns (by adjusting blade shape[7]) in a rapid manner.

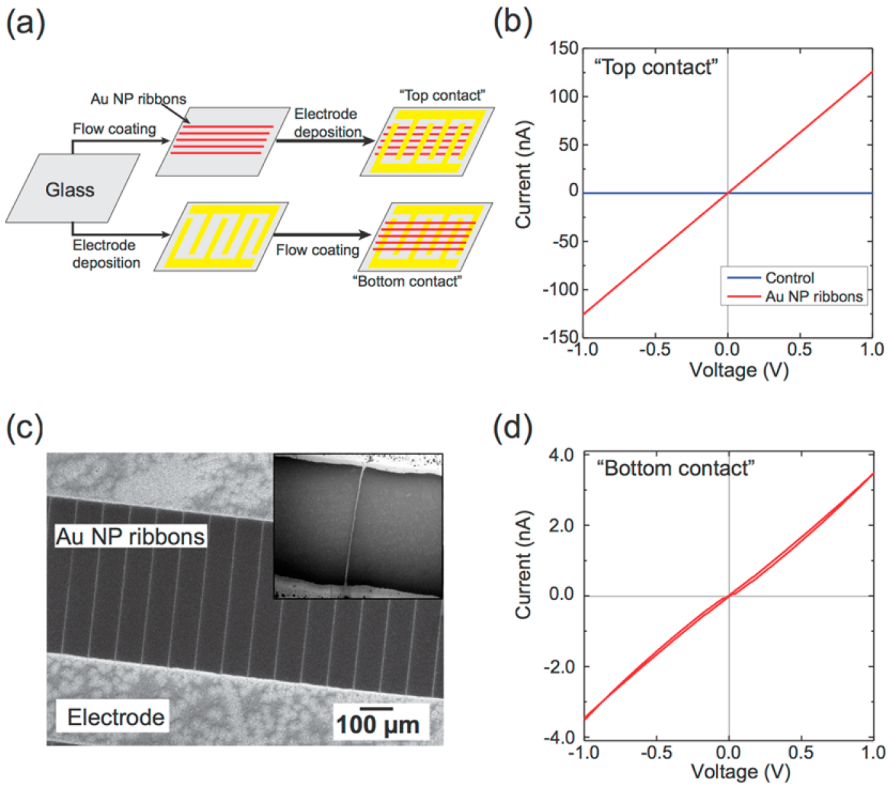

Figure 4. (a) Schematic diagram of top- and bottom-contact device fabrication. (b) Current−voltage (I−V) characteristics of Au NP-1 ribbon arrays measured in a top contact device. I−V response from a dual sweep (red) indicated linear ohmic response of NP ribbon arrays across the potential window with no hysteresis. (c) SEM image of Au NP-1 ribbons on interdigitated electrodes (bottom contact device). Inset: a 100 μm long Au NP-1 ribbon bridging two electrodes. (d) The I−V characteristic of a Au NP-1 ribbon array measured on a bottom contact device.

We next examined whether Au NP ribbons, prepared by flow coating from hydrophobic NPs such as **Au NP-1**, exhibit measurable conductivity, as they should if the NPs are spaced closely.[14] The literature describes a dependence of the Au NP conductivity on ligand chain length, in support of a distance-dependent electron-hopping mechanism in Langmuir monolayers of alkanethiol-stabilized Au NPs.[28] However, reports of alkanethiol functionalized Au NP monolayers vary considerably with respect to measured conductivity values. One report describes no detectable current from Langmuir-Schaeffer layers of dodecanethiol stabilized Au NPs,[29] while several studies reported the conductivity of dodecanethiol stabilized Au NP monolayers to be 10^{-5} S/m.[13,16,30] Alkyl ligand length dictates the outcome of these measurements – films of Au NPs with shorter ligands have shorter inter-NP distance and exhibit higher conductivity. Chen *et al.* reported the ohmic conductivity of *n*-butanethiol stabilized Au NPs on the order of 10^{-1} S/m, depending on the inter-NP distance reached upon compression (the monolayer is not conductive at inter-NP distances larger than 2.5 nm).[30] We note that all conductivity studies mentioned above used Au NPs synthesized by the two-phase method,[14] in which the variable results might be attributed to variable amounts of cationic surfactant ligand (TOAB).[31,32]

To measure the conductivity of **Au NP-1** ribbons, we prepared two interdigitated electrode (IDE) configurations, top-contact and bottom-contact, by shadow mask lithography (Figure 4a). In the top-contact configuration, **Au NP-1** ribbons were prepared by flow coating on glass, then covered with a lithography mask. Electrical contacts were introduced by evaporation of gold (electrode thickness: 100 nm) through the mask. In the bottom-contact device, the gold electrode configuration was first evaporated on glass (electrode thickness: 50 nm), followed by application of **Au NP-1** ribbons by flow coating over the electrodes. 500 Au NP ribbons were drawn between IDE fingers in each configuration, giving a sufficiently high current response for measuring conductivity, therefore reducing the impact of structural defects in any one line. We set the potential window at 2 V (−1 to 1 V), so as to avoid undesirable effects such as electrical sintering. The average ohmic response (I−V curve) of the Au NP ribbon samples (at least 6 samples per category) was measured using the two-point probe method, and these are the values we report for conductivity. The four-point method was also employed to verify the two-point results, with little difference in conductivity noted between the two types of measurements. As shown in Figure 4b, the top-contact configuration displayed a linear current−voltage (IV) response,

without hysteresis on dual sweep. The current response was noise free at a voltage sweep rate of 10 mV/s. The measured conductivity was 0.87 ± 0.3 S/m, calculated from: $\sigma = L/(N \times A \times R_{meas})$ using the values of measured resistance (R_{meas} = 8.0 × 10^6 ohm), cross-sectional area of the Au NP ribbons obtained from AFM analysis (A = 2.0 × 10^{-14} m^2), distance between each IDE finger (L = 7.0 × 10^{-5} m), and number of ribbons between IDE fingers (N = 500). Control measurements made by placing one probe on an area between Au NP-1 ribbons did not produce any current response, confirming that the ribbons are responsible for the observed conductivity. SEM analysis and conductivity measurements of Au NP-1 ribbons prepared in a bottom-contact configuration suggests conformal deposition of Au NPs as continuous ribbon arrays on the 3D structure (Figure 4c,d), with the ribbons bridging the electrodes, spanning a 500 μm gap that is 50 nm deep. Au NP-1 ribbons prepared in a bottom contact configuration on glass were visualized by electrically connecting the SEM sample mount to one of the gold electrodes. The SEM image in Figure 4c shows a conductive pathway between Au NP-1 ribbons and the underlying gold electrode. We speculate that the slightly nonlinear IV response (tunneling effect) (Figure 4d) and conductivity decrease (5.0 ± 3 × 10^{-2} S/m) of this bottom-contact device were due to increased inter-NP distance at the edge of the electrodes. Electrical characterization using conductive AFM, by physical attachment of a gold plate and AFM probe onto the ribbons, yielded lower conductivity values (3.3 × 10^{-2} S/m, see the Supporting Information, Figure SI-1). Top-contact devices exhibit higher conductivity because high interfacial contact is achieved as the gold electrode is evaporated continuously onto the Au NP ribbons, permitting interlayer penetration.

We also examined the effect of ligand binding groups on the conductivity of Au NP ribbons by comparing samples prepared from dodecylamine-[22] (**Au NP-4**, 3.3 ± 0.7 nm, ligand coverage: 7.2 ligands/nm^2), and dodecanethiol-covered Au NPs (**Au NP-1**). Dodecylamine and dodecanethiol have similar alkyl chain length, but amines bind less strongly to the gold surface than thiols. However, since prior reports suggest that the electronic properties of amine-functionalized Au films are more conductive than thiol-functionalized ones,[33,34] we included dodecylamine Au NPs in our Au NP ribbon formation and characterization.

Au NP-4 ribbons (two-point probe, top contact configuration) showed linear ohmic behavior without hysteresis, and conductivity values of (33 ± 15 S/m), about 2 orders of magnitude higher than **Au NP-1** ribbons (Figure 5). Four-point probe measurements showed the conductivity of **Au NP-4** ribbons (56 S/m) to be similar to the commercial conducting polymer PEDOT:PSS (~40 S/m).[35] The better electrical

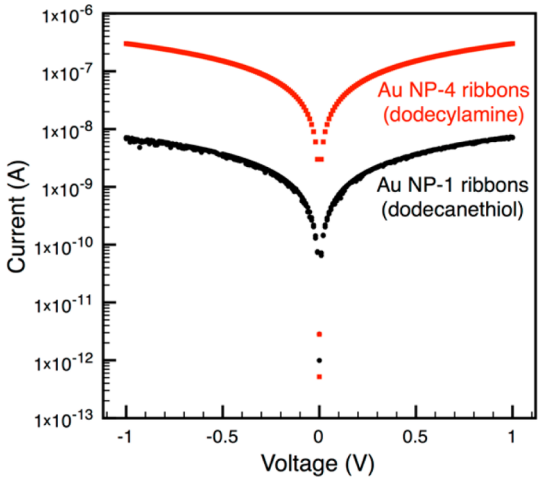

Figure 5. Nominal current−voltage response of Au NP ribbons prepared from dodecylamine-covered Au NPs (red) and dodecanethiol-stabilized Au NPs (black).

performance of amine-functionalized NPs compared to their thiol counterparts is thought to be due to more efficient electronic coupling of the nitrogen lone pair to the Au surface through a hybrid wave function formed along the metal−ligand bond axis.[33,34] For example, Parsons *et al.* reported that for ligands with alkyl chain lengths of 6−18 carbon, the conductivity of an alkylamine covered Au NP monolayer was approximately 2 orders of magnitude higher than the Au NP monolayer prepared from alkanethiol stabilized Au NPs.[36] Thus, our results agree with previous studies and extend the importance of this concept to the electrical properties of Au NP ribbon assemblies.

Many nanoparticle-based applications benefit from removal of organics (*i.e.*, ligands) to avoid resistive losses and to make the deposited layer insoluble. However, since the as-deposited NP ribbons have significant inter-NP voids, a porous structure results from thermal annealing, and the conductivity of **Au NP-1** and **Au NP-4** ribbons decreases after thermal annealing (150−240 °C). Attempts to sinter Au NP ribbons by microwave or UV irradiation created defects, giving inconsistent results in measured conductivity. Thus, inspired by reports of Ho and co-workers on Au NP-PEDOT films,[37] we added a trace amount of thiol-terminated polystyrene (**PS**, Mn: 5k, PDI: 1.2) to **Au NP-4** in toluene (**Au NP-5**, Au:PS = 9:1 v/v, [Au $NP_{5\ nm}$] = 1.3 μM, [PS_{5k}] = 1.2 μM) and used this mixture in flow coating to obtain Au-PS nanocomposite ribbons. The conductivity of the deposited **Au NP-5** ribbons was lower than **Au NP-4** ribbons due to the presence of polystyrene, an insulating polymer. However, upon annealing at 240 °C for 5 min, the conductivity of **Au NP-5** ribbons increased dramatically to 10^5 S/m (Figure 6a), similar to typical conductivity values for thermally sintered conductive adhesives prepared from micrometer-sized metal particles. We note that this process is reliable and reproducible:

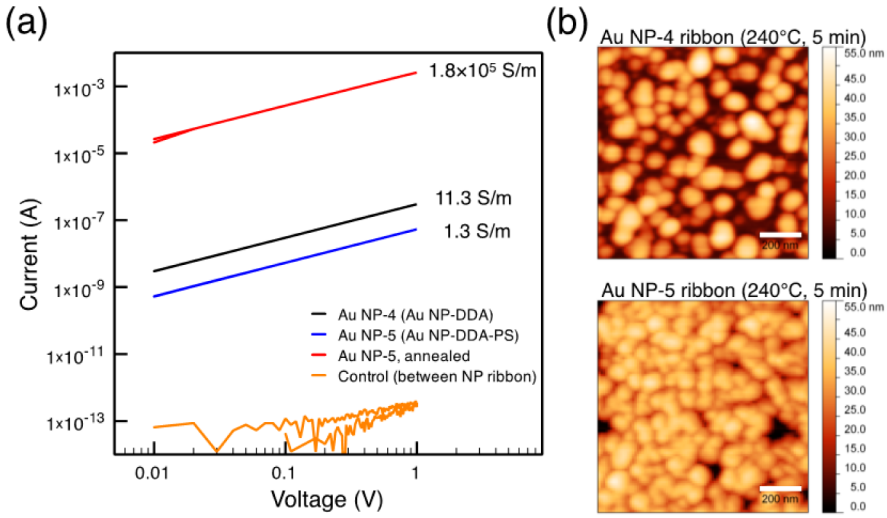

Figure 6. (a) Log−log plot of current−voltage response of Au NP-4 ribbons (black) and Au NP-5 ribbons before (blue) and after (red) annealing at 240 °C for 5 min. (b) AFM images of Au NP-4 ribbon (top) and Au NP-5 ribbon (bottom) after thermal annealing (240 °C, 5 min). Scale bars are 200 nm.

NP ribbons, irrespective of annealing before or after electrode deposition, showed similar conductivity ($1.4 \pm 0.6 \times 10^5$ S/m, from all six of the measured devices), confirming the versatility of this approach. NP ribbons with similar conductivity were also obtained when polystyrene (no chain-end thiol) was used as an additive (see the Supporting Information). In agreement with the report of Ho and co-workers,[37] we regard polystyrene as a "molecular filler" that acts to retard NP coalescence, control percolation, and prevent microcracks that would reduce conductivity. This is supported by AFM analysis: isolated NP aggregates were seen in **Au NP-1** ribbons and **Au NP-4** ribbons after annealing (240 °C, 5 min), while **Au NP-5** ribbons maintained interconnected paths after exposure to identical annealing conditions (Figure 6b).

CONCLUSIONS

We have demonstrated a method to fabricate high-resolution, conductive Au NP ribbon arrays over multiple length scales, giving new conductive structures having the unique combination of nanoscale height, submicrometer width, and centimeter length. High-quality Au NP ribbons were best prepared from the least polydisperse Au NP samples, synthesized by a surfactant free-one phase method. The linear ohmic response of Au NP ribbon arrays strongly suggested the presence of a continuous conductive path along the ribbon length. Conductivity measurements and SEM analysis showed that Au NP ribbons can tolerate surface roughness and maintain their electrical connectivity. Moreover, the conductivity of Au NP ribbons was increased by using dodecylamine covered Au NPs, and highly conductive Au NP ribbons were prepared by annealing Au NP-polystyrene nanocomposite ribbons. The use of ligands with different binding groups can increase the conductivity of NP ribbons, but highly conductive structures were only achieved by sintering nanocomposite structures containing a polymer additive. Thus, in this first report of Au NP ribbon arrays prepared from hydrophobic Au NPs, we showed an efficient and template free method to prepare conductive Au NP ribbon arrays (1−10 ribbons/s) over multiple length scales, thus providing a new platform approach to such unique, functional nanostructured materials.

METHODS

Chemicals and solvents were purchased form Sigma-Aldrich unless specified otherwise. Dodecanethiol-stabilized Au NPs were prepared by the one-phase and two-phase methods, as described in the Supporting Information. The Au NPs were purified by washings with mixtures of $CHCl_3$ and acetone, followed by centrifugation−redispersion cycles.[29] The flow coating process was conducted according to the protocol described in our previous work with slight modification.[7] The blade, consisting of flexible PET film (thickness: 80 μm, width: 2.5 cm), was scored at 1.2 mm from the edge, creating a hinge and constant capillary region parallel to the substrate. The coating blade was positioned 40° from horizontal surface, and the capillary region of the blade was positioned 5 μm above the substrate. The Au NP solution in toluene (1.0 mg/mL, [Au $NP_{5\ nm}$] = 1.3 μM, 5 μL) was injected slowly to fill the capillary opening between the blade and substrate. Once the solution was held by capillary forces under the blade, the stage was translated at a velocity of 1.5 mm/s, with a 100−1000 ms stopping time, giving a ribbon spacing of 30 μm. The stage translation was controlled from a computer interface based on LabView (National Instruments, Austin, TX). Top-contact and bottom-contact devices were made by evaporating 100 nm of gold (Kurt J. Lesker, 99.9999%) on a metal-mask covered glass substrate (Fisher Scientific). Conductivity measurements were carried out using the two-probe (500 Au NP ribbons, Keithley 4200-SCS, −1 to 1 V, 10 mV/s) and four-probe method (4 equally distanced (50 μm) electrodes (thickness: 100 nm) evaporated on 30 Au NP ribbons, fixed current, Keithley 4200-SCS).

Conflict of Interest: The authors declare no competing financial interest.

Acknowledgment. We acknowledge financial support from the Army Research Office (W911NF-11-1-0396) and the National Science Foundation Center for Hierarchical Manufacturing (CMMI-1025020). Facilities support from the NSF-Materials Research Science and Engineering Center (MRSEC) on Polymers is also acknowledged (MRSEC 0820506, DBI 0923105). We thank Dr. J. Hirsch for assistance with XPS measurements.

Supporting Information Available: Details on the synthesis and characterization of Au NP samples (TGA, XPS, TEM) and Au NP ribbons (conductivity, AFM). This material is available free of charge *via* the Internet at http://pubs.acs.org.

REFERENCES AND NOTES

1. Huang, J.; Kim, F.; Tao, A.; Connor, S.; Yang, P. Spontaneous Formation of Nanoparticle Stripe Patterns Through Dewetting. *Nat. Mater.* **2005**, *4*, 896–900.
2. Hong, S.; Zhu, J.; Mirkin, C. Multiple Ink Nanolithography: Toward a Multiple-Pen Nano-Plotter. *Science* **1999**, *286*, 523–525.
3. Park, J.-U.; Hardy, M.; Kang, S. J.; Barton, K.; Adair, K.; Mukhopadhyay, D. K.; Lee, C. Y.; Strano, M. S.; Alleyne, A. G.; Georgiadis, J. G.; *et al.* High-Resolution Electrohydrodynamic Jet Printing. *Nat. Mater.* **2007**, *6*, 782–789.
4. Tien, J.; Nelson, C.; Chen, C. Fabrication of Aligned Microstructures with a Single Elastomeric Stamp. *Proc. Natl. Acad. Sci. U.S.A.* **2002**, *99*, 1758–1762.
5. Bigioni, T.; Lin, X.; Nguyen, T.; Corwin, E.; Witten, T.; Jaeger, H. Kinetically Driven Self Assembly of Highly Ordered Nanoparticle Monolayers. *Nat. Mater.* **2006**, *5*, 265–270.
6. Kim, H. S.; Lee, C. H.; Sudeep, P. K.; Emrick, T.; Crosby, A. J. Nanoparticle Stripes, Grids, and Ribbons Produced by Flow Coating. *Adv. Mater.* **2010**, *22*, 4600–4604.
7. Lee, D. Y.; Pham, J. T.; Lawrence, J.; Lee, C. H.; Parkos, C.; Emrick, T.; Crosby, A. J. Macroscopic Nanoparticle Ribbons and Fabrics. *Adv. Mater.* **2013**, *25*, 1248–1253.
8. Daniel, M.; Astruc, D. Gold Nanoparticles: Assembly, Supramolecular Chemistry, Quantum-Size-Related Properties, and Applications Toward Biology, Catalysis, and Nanotechnology. *Chem. Rev.* **2004**, *104*, 293–346.
9. Diao, J.; Sun, J.; Hutchison, J.; Reeves, M. Self Assembled Nanoparticle Wires by Discontinuous Vertical Colloidal Deposition. *Appl. Phys. Lett.* **2005**, *87*, 103113.
10. Kakefuda, Y.; Narita, K.; Komeda, T.; Yoshimoto, S.; Hasegawa, S. Synthesis and Conductance Measurement of Periodic Arrays of Gold Nanoparticles. *Appl. Phys. Lett.* **2008**, *93*, 163103.
11. Farcau, C.; Moreira, H.; Viallet, B.; Grisolia, J.; Ressier, L. Tunable Conductive Nanoparticle Wire Arrays Fabricated by Convective Self-Assembly on Nonpatterned Substrates. *ACS Nano* **2010**, *4*, 7275–7282.
12. Brust, M.; Walker, M.; Bethell, D.; Schiffrin, D.; Whyman, R. Synthesis of Thiol-Derivatized Gold Nanoparticles in a 2-Phase Liquid-Liquid System. *J. Chem. Soc., Chem. Commun.* **1994**, 801–802.
13. Terrill, R.; Postlethwaite, T.; Chen, C.; Poon, C.; Terzis, A.; Chen, A.; Hutchison, J.; Clark, M.; Wignall, G.; Londono, J.; *et al.* Monolayers in Three Dimensions: NMR, SAXS, Thermal, and Electron Hopping Studies of Alkanethiol Stabilized Gold Clusters. *J. Am. Chem. Soc.* **1995**, *117*, 12537–12548.
14. Chen, S. Langmuir Monolayers of Gold Nanoparticles: From Ohmic to Rectifying Charge Transfer. *Anal. Chim. Acta* **2003**, *496*, 29–37.
15. Hardy, N. J.; Hanwell, M. D.; Richardson, T. H. Temperature Effects on the Electrical Conductivity of Thiol Encapsulated Gold Nanoparticle Thin Films. *J. Mater. Sci.: Mater. Electron.* **2007**, *18*, 943–949.
16. Snow, A.; Wohltjen, H. Size-Induced Metal to Semiconductor Transition in a Stabilized Gold Cluster Ensemble. *Chem. Mater.* **1998**, *10*, 947–949.
17. Zheng, N.; Fan, J.; Stucky, G. One-Step One-Phase Synthesis of Monodisperse Noble-Metallic Nanoparticles and Their Colloidal Crystals. *J. Am. Chem. Soc.* **2006**, *128*, 6550–6551.
18. Hiramatsu, H.; Osterloh, F. A Simple Large-Scale Synthesis of Nearly Monodisperse Gold and Silver Nanoparticles with Adjustable Sizes and with Exchangeable Surfactants. *Chem. Mater.* **2004**, *16*, 2509–2511.
19. Diao, J.; Qiu, F.; Chen, G.; Reeves, M. Surface Vertical Deposition for Gold Nanoparticle Film. *J. Phys. D: Appl. Phys.* **2003**, *36*, L25–L27.
20. Murray, C.; Norris, D.; Bawendi, M. Synthesis and Characterization of Nearly Monodisperse Cde (E = S, Se, Te) Semiconductor Nanocrystallites. *J. Am. Chem. Soc.* **1993**, *115*, 8706–8715.
21. Peng, Z.; Peng, X. Nearly Monodisperse and Shape-Controlled CdSe Nanocrystals *via* Alternative Routes: Nucleation and Growth. *J. Am. Chem. Soc.* **2002**, *124*, 3343–3353.
22. Polavarapu, L.; Xu, Q.-H. A Simple Method for Large Scale Synthesis of Highly Monodisperse Gold Nanoparticles at Room Temperature and Their Electron Relaxation Properties. *Nanotechnology* **2009**, *20*, 185606.
23. Fournier, J. B.; Cazabat, A. M. Tears of Wine. *EPL (Europhys. Lett.)* **1992**, *20*, 517–522.
24. Cazabat, A. M.; Heslot, F.; Troian, S. M.; Carles, P. Fingering Instability of Thin Spreading Films Driven by Temperature Gradients. *Nature* **1990**, *346*, 824–826.
25. Carney, R. P.; Kim, J. Y.; Qian, H.; Jin, R.; Mehenni, H.; Stellacci, F.; Bakr, O. M. Determination of Nanoparticle Size Distribution Together with Density or Molecular Weight by 2D Analytical Ultracentrifugation. *Nat. Commun.* **2011**, *2*, 1–8.
26. Garbin, V.; Crocker, J. C.; Stebe, K. J. Forced Desorption of Nanoparticles From an Oil−Water Interface. *Langmuir* **2011**, *28*, 1663–1667.
27. Rowe, M.; Plass, K.; Kim, K.; Kurdak, C.; Zellers, E.; Matzger, A. Single-Phase Synthesis of Functionalized Gold Nanoparticles. *Chem. Mater.* **2004**, *16*, 3513–3517.
28. Chan, Y.-T.; Li, S.; Moorefield, C. N.; Wang, P.; Shreiner, C. D.; Newkome, G. R. Self-Assembly, Disassembly, and Reassembly of Gold Nanorods Mediated by Bis(Terpyridine)-Metal Connectivity. *Chem.—Eur. J.* **2010**, *16*, 4164–4168.
29. Hanwell, M. D.; Heriot, S. Y.; Richardson, T. H.; Cowlam, N.; Ross, I. M. Gas and Vapour Sensing Characteristics of Langmuir-Schaeffer Thiol Encapsulated Gold Nanoparticle Thin Films. *Colloids Surf., A* **2006**, *284*, 379–383.
30. Wuelfing, W.; Green, S.; Pietron, J.; Cliffel, D.; Murray, R. Electronic Conductivity of Solid-State, Mixed-Valent, Monolayer-Protected Au Clusters. *J. Am. Chem. Soc.* **2000**, *122*, 11465–11472.
31. Waters, C.; Mills, A.; Johnson, K.; Schiffrin, D. Purification of Dodecanethiol Derivatised Gold Nanoparticles. *Chem. Commun.* **2003**, 540–541.
32. Thierry, B.; Ng, J.; Krieg, T.; Griesser, H. J. A Robust Procedure for the Functionalization of Gold Nanorods and Noble Metal Nanoparticles. *Chem. Commun.* **2009**, 1724–1726.
33. Venkataraman, L.; Klare, J.; Tam, I.; Nuckolls, C.; Hybertsen, M.; Steigerwald, M. Single-Molecule Circuits with Well-Defined Molecular Conductance. *Nano Lett.* **2006**, *6*, 458–462.
34. Fagas, G.; Greer, J. C. Tunnelling in Alkanes Anchored to Gold Electrodes *via* Amine End Groups. *Nanotechnology* **2007**, *18*, 424010.
35. Ouyang, B.; Chi, C.; Chen, F.; Xi, Q.; Yang, Y. High-Conductivity Poly (3,4-Ethylenedioxythiophene): Poly(Styrene Sulfonate) Film and Its Application in Polymer Optoelectronic Devices. *Adv. Funct. Mater.* **2005**, *15*, 203–208.
36. Chu, C.; Na, J.-S.; Parsons, G. N. Conductivity in Alkylamine/Gold and Alkanethiol/Gold Molecular Junctions Measured in Molecule/Nanoparticle/Molecule Bridges and Conducting Probe Structures. *J. Am. Chem. Soc.* **2007**, *129*, 2287–2296.
37. Sivaramakrishnan, S.; Chia, P.-J.; Yeo, Y.-C.; Chua, L.-L.; Ho, P. K.-H. Controlled Insulator-to-Metal Transformation in Printable Polymer Composites with Nanometal Clusters. *Nat. Mater.* **2007**, *6*, 149–155.